CNN-based vane-type vortex generator modelling

Koldo Portal-Porras, Unai Fernandez-Gamiz, Ekaitz Zulueta, Roberto Garcia-Fernandez & Xabier Uralde-Guinea

Published online: 05 Jan 2024.

Submit your article to this journal ↗

Article views: 175

View related articles ↗

View Crossmark data ↗

Taylor & Francis
Taylor & Francis Group

CNN-based vane-type vortex generator modelling

Koldo Portal-Porras[a], Unai Fernandez-Gamiz[a], Ekaitz Zulueta[b], Roberto Garcia-Fernandez[a,c] and Xabier Uralde-Guinea[a]

[a]Nuclear Engineering and Fluid Mechanics Department, University of the Basque Country, UPV/EHU, Vitoria-Gasteiz, Spain; [b]System Engineering and Automation Control Department, University of the Basque Country, UPV/EHU, Vitoria-Gasteiz, Spain; [c]Sunsundegui S.A., Altsasu, Navarra

ABSTRACT

The simplicity and accuracy of Computational Fluid Dynamics (CFD) tools have made them the most widely used method for solving fluid dynamics problems. However, these tools have some limitations, being the most significant the required computational resources. This fact, added to the growth of the Artificial Intelligence, has led to an increasing number of studies using data-driven methods to solve fluid dynamic problems. Flow control devices are a very popular research topic, since their implementation can significantly improve the behaviour of the flow. Among these devices, Vortex Generators (VGs) can be highlighted for their simplicity, efficiency and numerous applications. In this study, a Convolutional Neural Network (CNN) is proposed to predict the flow behaviour on the wake behind VGs. In order to obtain data for training the network, 20 different CFD simulations were conducted, considering the same inflow conditions but different vane heights and angles of attack of the VGs. The results show that the CNN is able to accurately predict the velocity and vorticity fields on the wake of the VG, being the most conflictive cases the ones with tall VGs, large angles of attack and close distances to the VGs. Additionally, the vortical structure, vortex path and velocity profiles on the vortex core of the main vortex are evaluated, showing good agreements with CFD results.

Introduction

Since their introduction, CFD tools have been one of the most common methods for solving fluid dynamic problems, due to their simplicity and capability to model the turbulence. However, CFD tools have certain limitations, which can be prohibitive. Among these limitations are the computational time and resources required to run the simulations, especially when working with very complex geometries or very accurate turbulence models; the influence of the user, most notably when meshing the domain, defining the numerical models, setting the conditions of the simulations, and many others. These aspects, added to the irruption of Deep Learning (DL) techniques, have led more and more authors to apply data-driven methods to solve fluid dynamic problems.

Initial efforts focused on obtaining predictions of the different fields in generic cases with simple geometries, in order to evaluate the capability of DL-based methods to make predictions with this kind of problems. Although there is a wide variety of architectures that can provide accurate predictions of flows around geometries, as stated by Zhang et al. (2018), CNNs offer the greatest generalisation capacity, since these networks allow introducing different geometries on a simple way. Guo et al. (2016) designed a CNN to predict pressure and velocity fields of steady-state laminar flows around simple geometries. Based in that study, Ribeiro et al. (2020) tested the accuracy of different CNN architectures for predicting laminar flows, obtaining a significant accuracy improvement. Portal-Porras et al. (2021b) proposed the implementation of a previous stage for predicting pressure and vorticity fields, in order to improve the predictions of a CNN of the velocity fields of turbulent flows. Kashefi et al. (2020) developed a PointNet (Qi et al., 2017) architecture for field prediction around irregular shapes, showing that the network is able to change its predictions with slight geometry modifications, which is essential for design optimisation. In all the mentioned studies the computational time is reduced between 3 and 5 order of magnitude in comparison with CFD simulations.

Based on the knowledge provided by the aforementioned studies and many others, more and more authors

are using this type of networks for real applications, such as aerfoils (Chen et al., 2020; Thuerey et al., 2020; Yilmaz & German, 2017), car aerodynamics (Jacob et al., 2022), thermal systems (Du et al., 2021), chemical reactions (Ren et al., 2021) and many others.

Within fluid dynamics, flow control devices, both active and passive, are a very popular research topic, since their implementation can lead to a great improvement of flow behaviour. In addition, there is a large variety of devices and there are many parameters that affect their behaviour, which makes their study more complex and challenging. Aramendia-Iradi et al. (2016) and Aramendia (2017) provided an exhaustive review of the available flow control devices.

Among flow control devices, VGs can be highlighted for their simplicity, efficiency and numerous applications. VGs are passive flow control devices, whose objective is to delay or remove the flow separation, transferring the energy generated from the outer region to the boundary layer region. They are small vanes, usually mounted in pairs, placed before the expected region of separation of the boundary layer with an incident angle with the oncoming flow. Although they are primarily triangular or rectangular, VGs can be of various shapes. Typically, the height of the VGs is similar to the boundary layer thickness in the location where the VG is implemented, aiming to ensure a good interaction between the boundary layer and the vortex generated by the VG. However, since tall VGs lead to high drag forces, in many applications VGs whose height is less than the boundary layer thickness, known as Sub-Boundary-Layer Vortex Generators (SBVG), are used, as in Ashill et al. (2001, 2002).

Traditionally, VGs, and passive flow control devices in general, have been studied by means of experimental tests or CFD simulations, such as in Ibarra-Udaeta et al. (2020), Urkiola et al. (2017), Portal-Porras et al. (2021a), Fernandez-Gamiz et al. (2012, 2016, 2018). However, with the advent of Deep Learning, a new possibility for the analysis and optimisation of these devices arised. Portal-Porras et al. (2022), by means of a CNN, predicted the velocity and pressure fields around two different flow control devices, microtabs and Gurney flaps, located on the Trailing Edge (TE) of an aerfoil. Additionally, in that study, lift and drag coefficients of the aerfoil with those devices are predicted using a variation of the proposed CNN.

Even if DL methods can be very useful for a fast and accurate prediction of flows, their main limitation is the prediction of three-dimensional flows; since, as stated by Kashefi et al. (2020), when working with three-dimensional CNNs, the high computational cost leads to low-resolution limited workspaces. For example, in the study conducted by Guo et al. (2016) a domain is divided into a 128×256 array for two-dimensional flows, while for three-dimensional flows the domain is divided into a $32 \times 32 \times 32$ array. This causes the predictions to be unreliable. If a small domain is selected, only the region close to the geometry can be displayed, losing characteristics of the flow. On the contrary, the selection of a large domain makes the representation of the geometry in the domain coarse, and therefore inadequate. For these reasons, in order to ensure the accuracy of the results and to reduce the required computational time and resources, alternatives for the prediction of three-dimensional flows using DL tools must be sought.

In the present paper the capability of a two-dimensional CNN to learn and predict three-dimensional flow phenomena of the wake behind SBVGs is evaluated, avoiding the use of computationally demanding three-dimensional CNNs. With this objective, a two-dimensional CNN is designed and trained to predict the velocity and vorticity fields in different planes located on the wake behind the SBVGs. For training the CNN, the results of 20 different CFD simulations are used, in which different vane heights and angles of attack of the VGs are considered.

The remainder of the manuscript is structured as follows: in 'Methodology' a detailed explanation of the methodology followed for setting up and conducting CFD simulations, and designing and training the proposed CNN is provided; in 'Results and Discussion' the predictions of the CNN in terms of velocity and vorticity fields, vortical structure, vortex path and velocity profiles of the core of the vortex are presented, and these predictions are compared with the CFD results; finally, in 'Conclusion' the main conclusions extracted from this study are explained.

Methodology

CFD setup

Aiming to obtain data to train, validate and test the CNN, 20 different simulations of vane-type VGs on a flat plate were conducted, considering different VG heights (H) and Angles of Attack (α) in each simulation. To conduct these simulations Star-CCM + v2019.1 commercial code was used.

In all the cases the computational domain consists of a block with a VG of its lower surface. The flow goes from the upstream part of the block to the downstream part; therefore, they are set as inlet and outlet, respectively. The surfaces of the VG and the lower surface of the block are set as no-slip walls, while the rest of the surfaces of the block are set as symmetry planes, in order to avoid affecting the flow. The dimensions of the block were
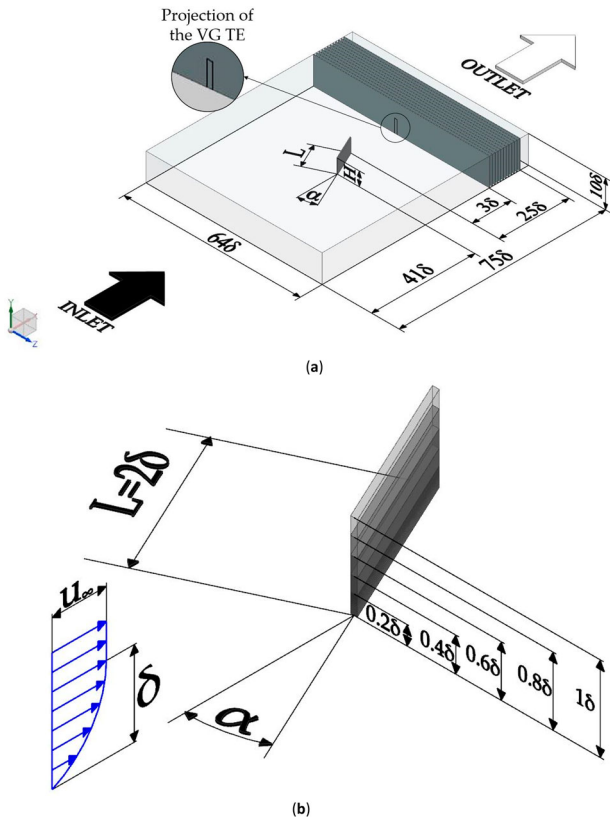
Figure 1. Dimensions of the numerical domain. (**a**) Numerical domain (not to scale); (**b**) VG dimensions and parameters.

Figure 2. Refined mesh around the VG for $H = 1\delta$.

Both mesh quality and mesh dependence have been thoroughly analysed in the previous studies conducted by Urkiola et al. (2017), Ibarra-Udaeta et al. (2020) and Portal-Porras et al. (2021a). Demonstrating that the used meshes are suitable for these simulations.

Regarding the fluid, incompressible turbulent flow in steady-state is considered. The Reynolds number (Re) based on the height of the VG is between 5400 and 27,000 according to Expression (1).

$$Re = \frac{u_\infty \cdot H}{\nu} \qquad (1)$$

where u_∞ refers to the freestream velocity of the flow, which is set at 20 m/s, and ν to the kinematic viscosity.

For turbulence modelling Menter's RANS-based k-ω Shear Stress Transport (SST) (Menter, 1993) turbulence model is selected. As demonstrated by Allan et al. (2002), in comparison with other RANS models, SST models provide more accurate results, especially in terms of vortex trajectory and streamwise peak vorticity. Therefore, this turbulence model is considered to be the most appropriate for the analysed problem.

Convolutional neural network

Input and output layers

As the considered computational domain is too large to be processed by the neural network, only the most important part of the planes is evaluated, i.e. the area where the vortices can be observed. This region is the one marked by a white rectangle in Figure 3.

In order to obtain more samples to train the network, a data augmentation procedure was followed. In this case, the procedure to increase the amount of data consisted in obtaining samples of the same area of interest but with a small offset of 5 or 10 cm on each side. These zones are the

defined to ensure that the boundary layer thickness (δ) at the location of the VG is equal to 0.25 m.

As the objective of the CFD simulations is to obtain different samples, 20 different VG configurations are considered, combining four different angles of attack, 10°, 12°, 15° and 18°; and five different VG heights, 0.2δ, 0.4δ, 0.6δ, 0.8δ and 1δ. The length of the VG is equal to 2δ in all the cases. For more information about the computational domain and VG dimensions check Figure 1.

For data extraction, 12 different planes located at the wake behind the VG are considered. These planes are located at a distance between 3δ and 25δ from the TE of the VG, being each plane distanced by 2δ from the others.

With the explained computational domain five different structured meshes of around 11 million cells were generated, one for each VG height. The normalised height of the cell closest to the wall ($\Delta z/\delta$) was set at 1.5 · 10^{-6} in all the cases. The procedure described by Urkiola et al. (2017) was followed to generate all the meshes. The meshes are more refined in the near-VG region, in order to obtain more accurate results in this region. The meshes were rotated depending on the case, in order to obtain the desired angle of attack. Figure 2 shows an example of the near-VG region of the mesh generated for $H = 1\delta$.
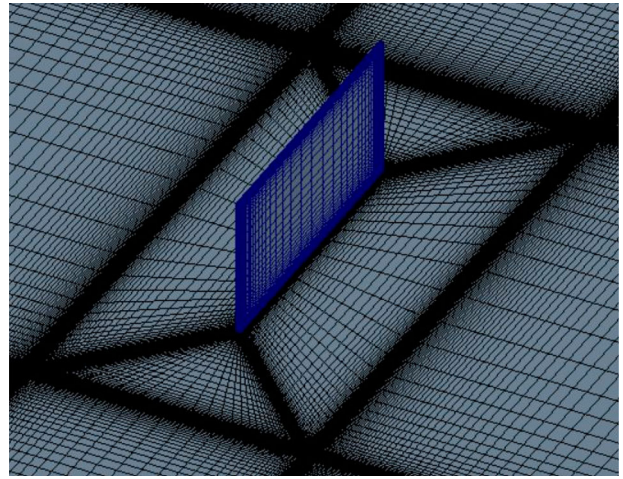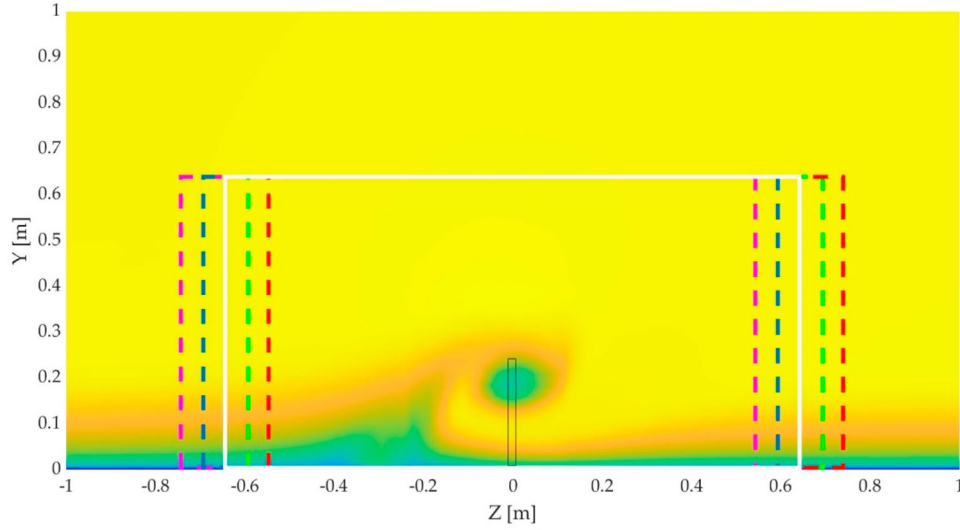
Figure 3. Area of interest of an example case. The white rectangle shows the area of interest for the baseline case and the purple-, blue-, green- and red-dashed rectangles show the areas of interest for the augmented cases.

purple, red, blue and green dashed rectangles of Figure 3. Additionally, the symmetrical cases in the Z-axis of all the samples were created, resulting in a total of 200 cases and 2400 planes, 12 per each case. Among these samples, the 240 samples corresponding to the baseline cases are considered to test the network, and the augmented dataset to train and validate it. The dataset only includes the explained samples, without considering stochasticity errors.

Two different layers are created to represent these regions. The first layer contains the projection of the TE of the VG, and the value of this projection is defined by the α of the VG. The rest of the layer defines the distance between the analysed plane and the TE of the VG. Therefore, this layer defines the location, height and angle of attack of the VG. The second layer contains a Signed Distance Function (SDF) that represents the minimum distance between the projection of the TE of the VG each point of the domain. Figure 4 shows an example of the generated layers.

To create the SDF layer firstly the zero-level set (Z) is created following Expression (2). This is the level of the plane where the contour of the projection of the TE is located. This set is marked with a white rectangle in Figure 4(b).

$$Z = \{(X, Y) \in R^2 / SDF(x, y) = 0\} \quad (2)$$

Then, the sign of SDF is defined. $SDF(x, y) = 0$ if (x,y) is on the geometry contour; $SDF(x, y) < 0$ if (x,y) is inside the geometry; and $SDF(x, y) > 0$ if (x,y) is outside the geometry.

Finally, the value of each element is calculated following Expression (3).

$$SDF(x, y) = \min_{(X,Y) \in Z} |(x, y) - (X, Y)| \cdot sign \quad (3)$$

To prepare the output layers, the obtained results of the CFD simulations are firstly interpolated to fit into 128×256 arrays. Then, each variable is normalised, following Expressions (4)–(7).

$$u_x^* = \frac{u_x}{u_\infty} \quad (4)$$

$$u_y^* = \frac{u_y}{u_\infty} \quad (5)$$

$$u_z^* = \frac{u_z}{u_\infty} \quad (6)$$

$$\omega_x^* = \frac{\omega_x \cdot \delta}{u_\infty} \quad (7)$$

where u_x^*, u_y^*, u_z^* and ω_x^* are the dimensionless variables.

Finally, all the input and output layers are ranged between 0 and 1 following Expression (8), aiming to speed up and enhance the training process.

$$\Phi' = \frac{\Phi - \min(\Phi)}{\max(\Phi) - \min(\Phi)} \quad (8)$$

where Φ is replaced by each dimensionless variable.

CNN architecture

In this study, a CNN is proposed to predict the velocity and vorticity fields on the wake behind the VGs. MATLAB (2022) commercial code with its Deep Learning Toolbox (2021) were used to design and train the network.
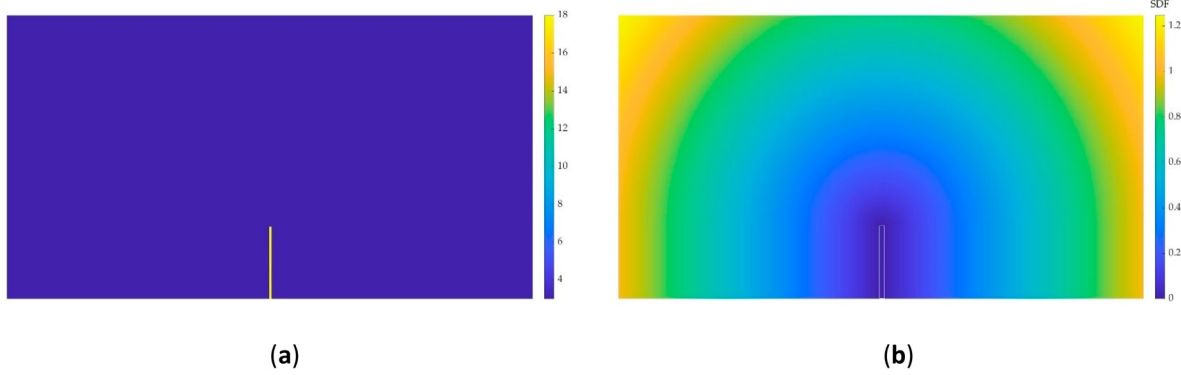
Figure 4. Input layers of the CNN for an example case. (**a**) Layer for defining the VG; (**b**) SDF layer.
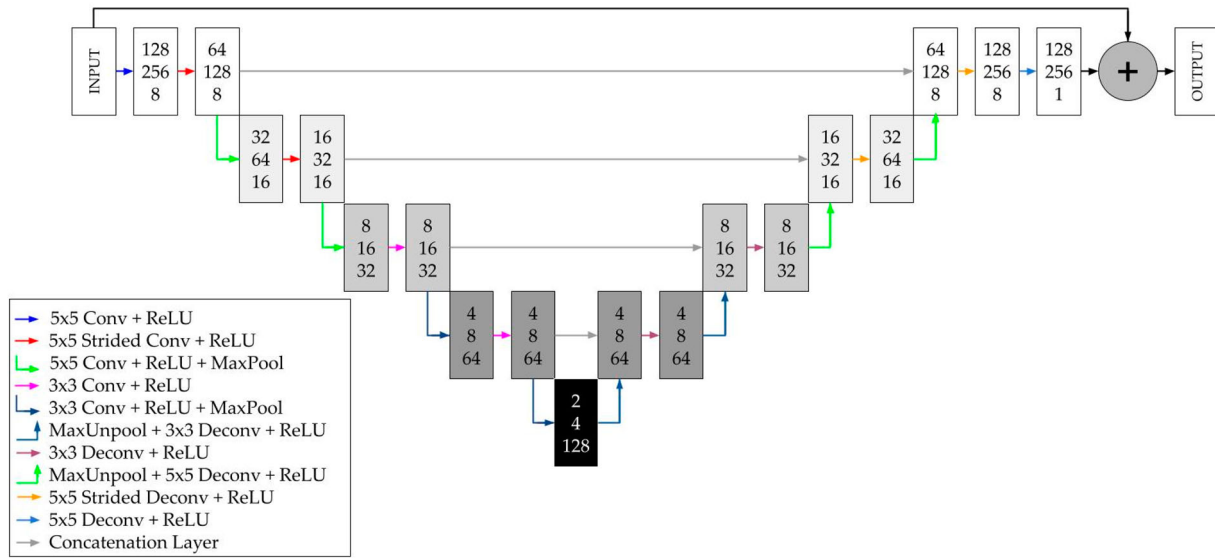

Figure 5. Schematic view of the proposed CNN.

Among the different architectures of CNNs available, an encoder–decoder architecture is selected, in particular a U-Net architecture (Ronneberger et al., 2015). This kind of network has been widely used to solve fluid-mechanical problems, as in Guo et al. (2016) and Thuerey et al. (2020). The proposed network consists of four encoder/decoder blocks. Each encoding block contains two convolutional layers, both of them followed by a ReLU (Rectifier Linear Unit) activation function layer. The second convolutional layer is also followed by a Max Pooling layer. In the first two encoding blocks strided convolutions are performed with a kernel of 5×5; and in the last two encoding blocks normal convolutions with a kernel of 3×3 are performed. The number of filters is doubled in each encoding block. The decoding part of the network performs the reverse process of the encoding part. Each encoding block is connected to its respective decoding block by means of concatenation layers. Figure 5 shows a schematic representation of the proposed CNN. Portal-Porras et al. (2021b, 2022)

successfully applied this network for velocity, vorticity and pressure prediction around simple geometries and aerfoil flow control devices, respectively.

For training the network Adam optimiser (Kingma & Ba, 2017) was used, with a learning rate of 0.001, a batch size of 64, and a weight decay of 0.005. From the dataset of 2400 samples, the previously-mentioned 240 samples are considered for network-testing, and the rest of the samples are split into 70% training and 30% validation. The validation was performed after each epoch.

Results and discussion

In order to determine the reliability of the proposed CNN for predicting flows on the wake behind VGs, the predictions of the velocity and vorticity fields obtained with the CNN are compared to the ones obtained with CFD simulations. Additionally, based on the velocity and vorticity fields, other features of the main vortex generated by the VGs are extracted, such as, vortical structure, velocity
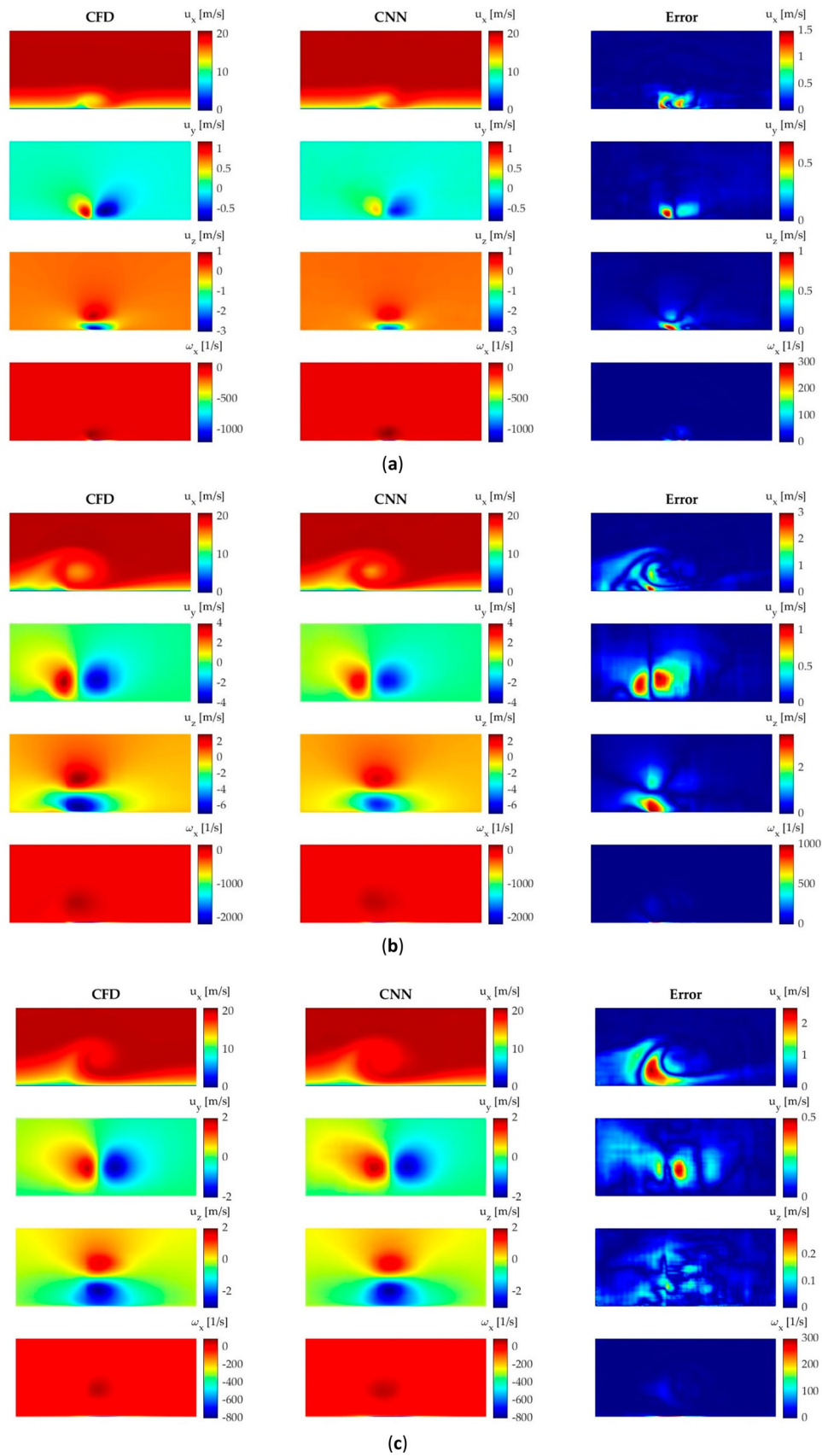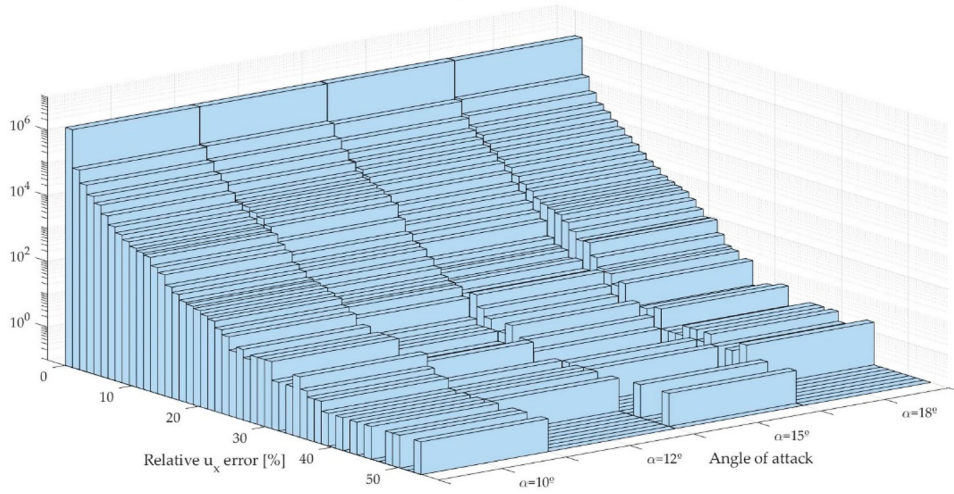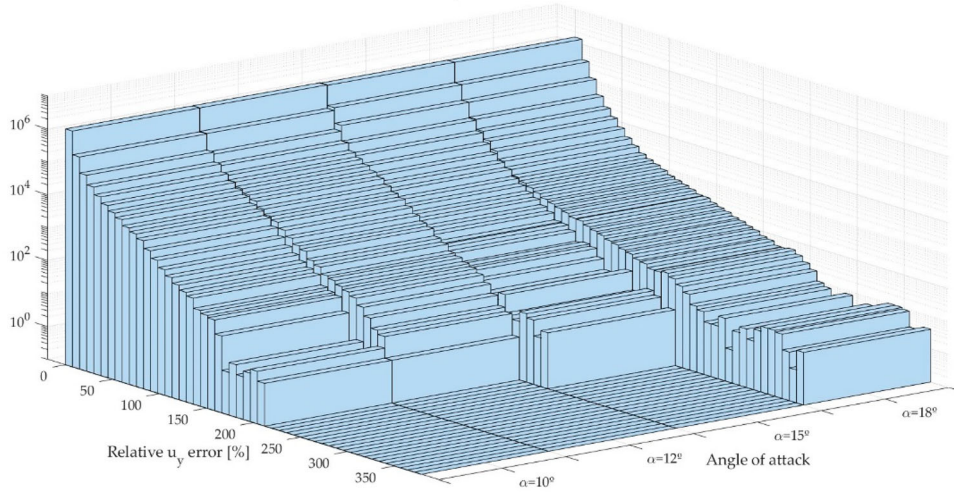
Figure 6. Comparison of the predictions obtained by CFD and CNN for three aleatory cases. (**a**) $H = 0.2\delta$, $\alpha = 12°$ and $x/\delta = 5$; (**b**) $H = 0.8\delta$, $\alpha = 18°$ and $x/\delta = 9$; (**c**) $H = 1\delta$, $\alpha = 10°$ and $x/\delta = 13$.
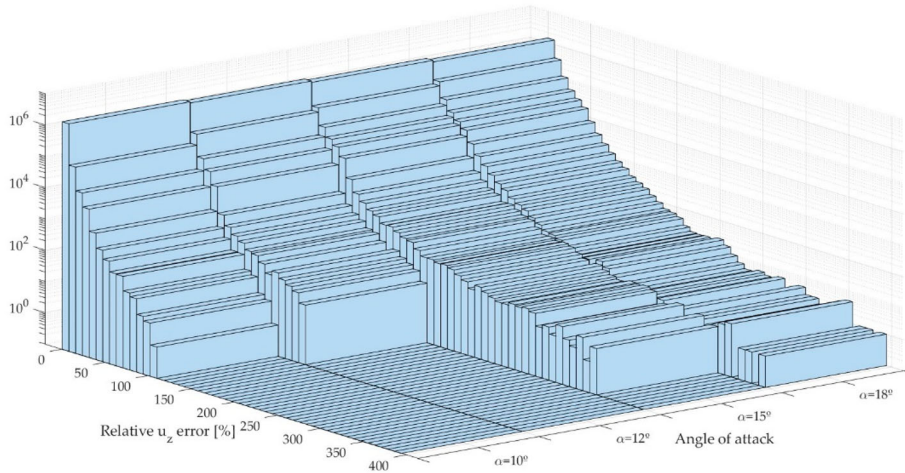
Figure 7. Relative error analysis based on the angle of attack of the VGs. (**a**) Relative u_x error; (**b**) Relative u_y error; (**c**) Relative u_z error; (**d**) Relative ω_x error.
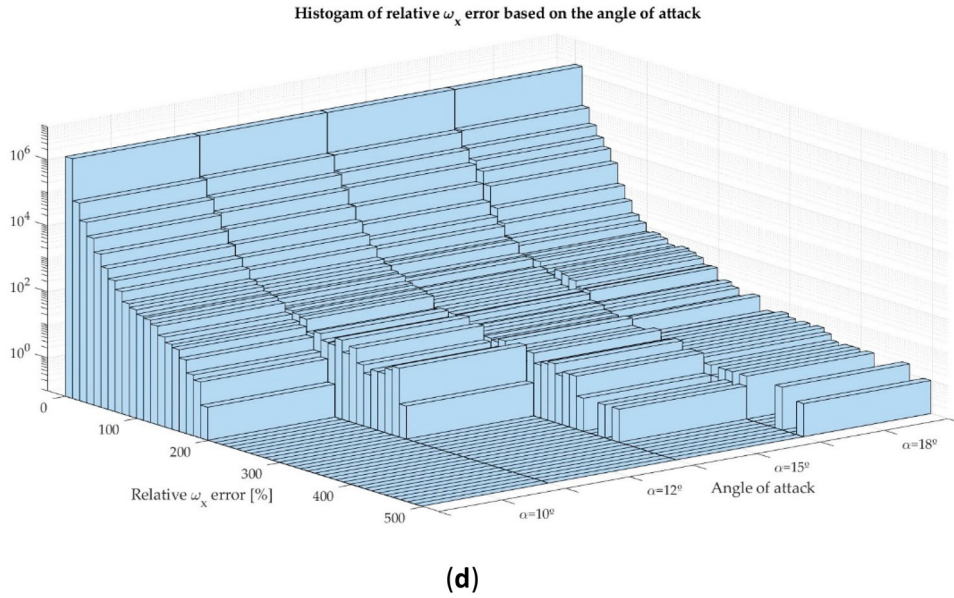
(d)

Figure 7. Continued.

Table 1. Arithmetic mean and standard deviation of the results obtained with CFD and CNN.

	CFD				CNN			
	u_x	u_y	u_z	ω_x	u_x	u_y	u_z	ω_x
Arithmetic mean (μ)	19.0355	−0.0142	−0.0956	−0.4123	19.0554	−0.0041	−0.0757	−0.123
Standard deviation (σ)	2.4349	0.5303	0.7795	39.7207	2.424	0.4774	0.6789	38.9628

profiles and vortex path. To conduct this comparison between CFD and CNN only the cases from the test-set are considered.

Velocity and vorticity fields

A comparison of the results of velocity and vorticity fields obtained with both methods is performed. To conduct this comparison three different random cases are considered, each one with a different vane-height, angle of attack and distance of the plane from the TE of the VG. Figure 6 shows this comparison and the error of the CNN predictions taking the CFD results as benchmark.

The velocity fields show that the CNN is able to accurately predict the shape of the vortexes generated by the VGs, predicting all the vortexes that compose the primary vortex mechanism described by Velte et al. (2016). The most troubleshooting area is the core of the primary vortex, where the CNN underestimates the y- and z-components of the velocity. Another troubleshooting area is the suction side of the horseshow vortex described by Velte et al. (2016), where the CNN undervalues the x-component of the velocity.

Regarding the vorticity, although the maximum errors are considerably high in all the cases evaluated, these errors appear in the near-wall region, where the vorticity

increases due to the influence of the boundary layer. However, the errors in the area of interest, i.e. in the area where the main vortex appears, are acceptable.

In order to obtain a quantitative view of the results, the arithmetic mean (μ) and standard deviation (σ) of the whole test-set are analysed. These values are presented in Table 1. The results of these parameters show that the values obtained with both methods are very similar, being the largest differences in the y and z components of the velocity.

Error analysis

An error analysis is carried out in order to evaluate which parameters most affect the CNN predictions. For this analysis the relative error (ε_R) of each of the magnitudes at all points predicted by the CNN is considered, calculated on the basis of the Expression 9. An adjusting scalar (k) is added on the denominator of this expression to avoid infinite relative errors when the CFD results are equal to zero. This scalar is equal to 0.01 for u_x and ω_x and 0.001 for u_y and u_z, in order to minimise its impact on the results.

$$\varepsilon_R = \frac{|x_{CFD} - x_{CNN}|}{|x_{CFD}| + k} \cdot 100 \tag{9}$$

where x is the value of each magnitude.
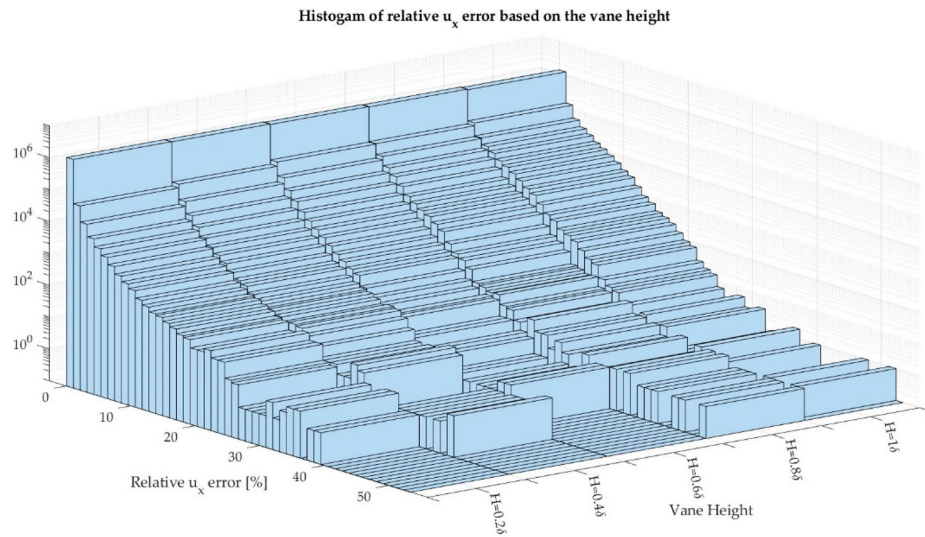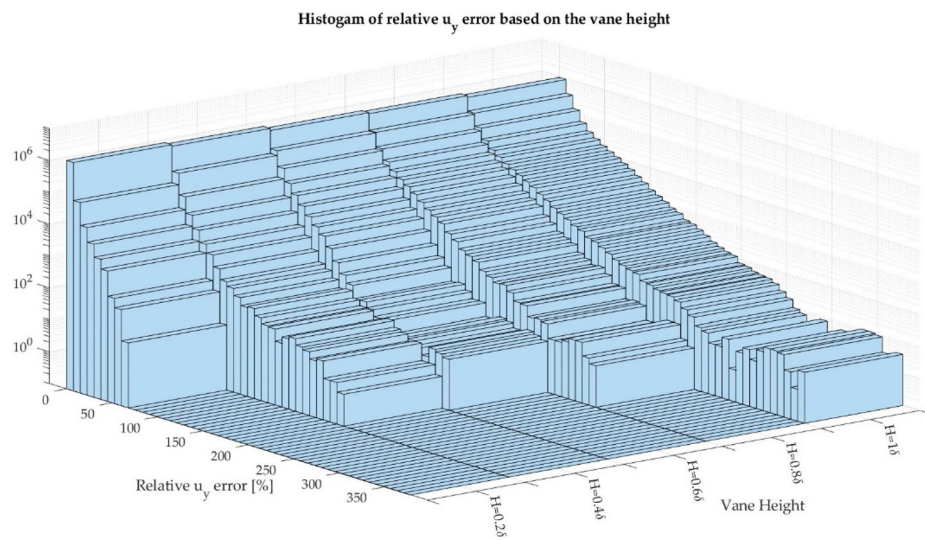
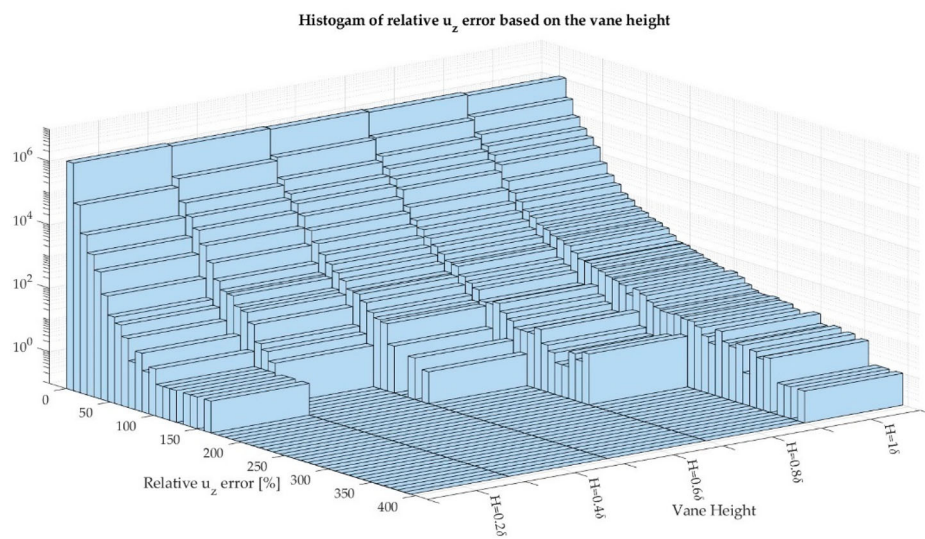**Figure 8.** Relative error analysis based on the vane height. (**a**) Relative u_x error; (**b**) Relative u_y error; (**c**) Relative u_z error; (**d**) Relative ω_x error.
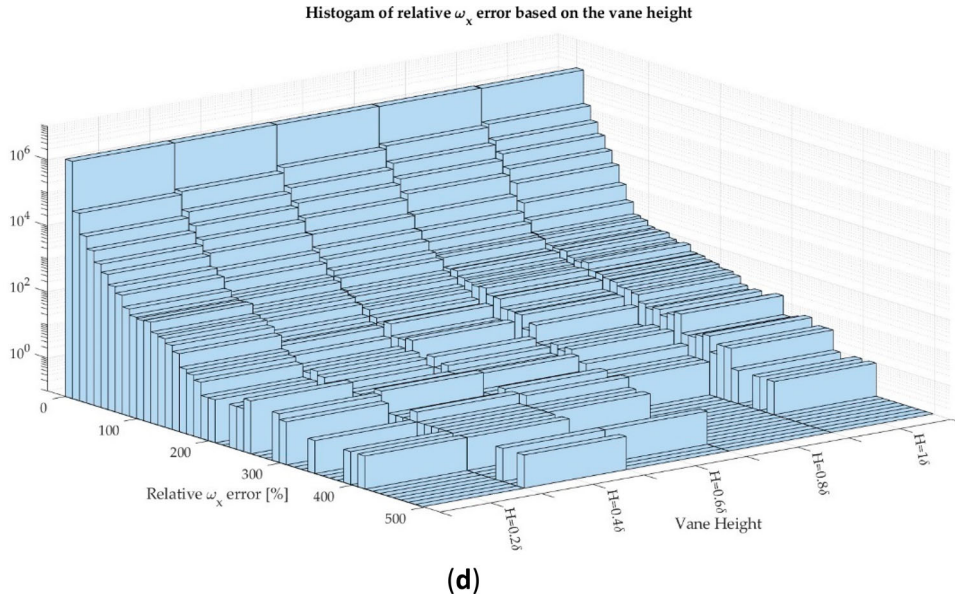
(d)

Figure 8. Continued.

Figure 7 displays the relative error analysis based on the angle of attack of the VGs; Figure 8 based on the vane height and Figure 9 based on the distance of the plane from the TE of the VG.

The comparison of the relative error based on the angle of attack of the VG shows that the largest angles of attack lead to the largest relative errors, most notably in u_y, u_z and ω_x. These three magnitudes show the rotation of the vortex. As the angle of attack increases, the strength and size of the vortex increases, and this makes the CNN predictions of the mentioned magnitudes worsen. In the case of u_x, even if the maximum errors are similar in all the cases, $\alpha = 18°$ is the case in which the medium-range errors appear the most.

The comparison of the relative error based on the vane height demonstrates that as the height of the VG decreases, the predictions of the three velocity components improve. As with the angle of attack, the higher VGs lead to bigger and stronger vortexes, which complicates the predictions of the CNN. In the case of ω_x, similar relative errors are found for all the VG heights.

The comparison of the relative error based on the distance from the TE of the VG shows that the largest relative errors appear on the near-wake region, and as the distance from the TE increases the relative errors decrease. This is attributed to the vortex structure, whose complexity decreases as it distances from the VG.

As shown in the histograms, some relative errors are considerably high. However, these errors appear in insignificant areas, such as the walls. In addition, the
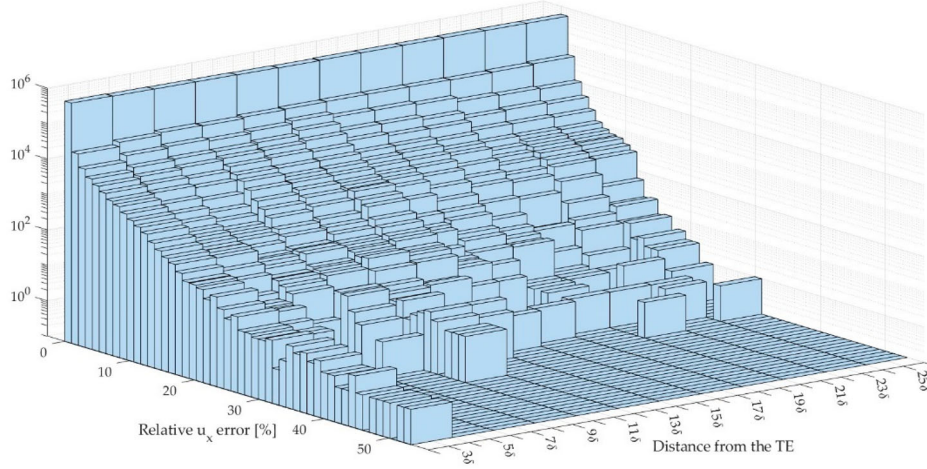
ground truth value where these errors appear is very close to zero, which makes the relative error increase.
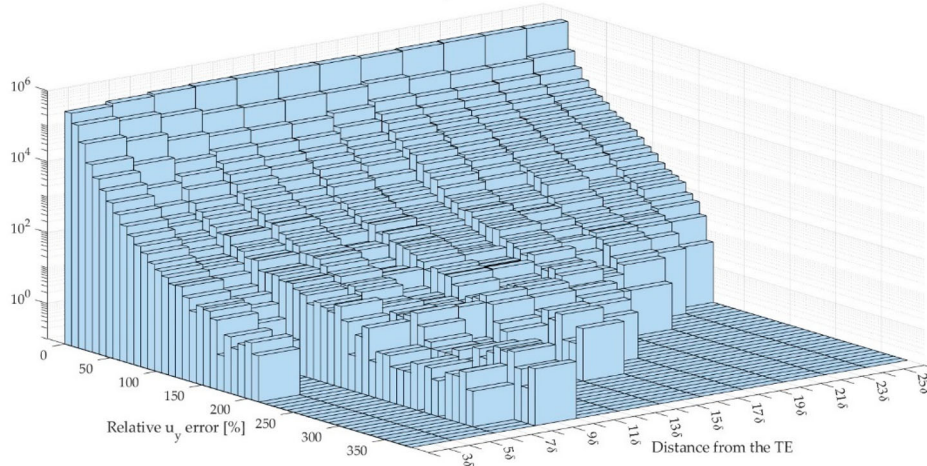
Vortical structure

In order to conduct a qualitative comparison of the vortical structure, the vortex core is considered. For this study, it is considered that the vortex core is the region where the vorticity is higher than the half of the peak vorticity ($\frac{\omega_{peak}}{2}$). Figure 10 shows the representation of the primary vortex at a distance of 5δ from the TE of the VG with both methods.

The results show that the size of the vortex increases as the vane-height and angle of attack increase. This increase is more noticeable with low vane-heights and high angles of attack. The vortices obtained with the highest VGs have a circular shape; and as the height of the VGs decreases, the shape of the vortices change, having the vortices obtained with the lowest VGs an elliptical shape, due to the boundary layer influence. As shown in more detail later in the article, the lateral displacement of the vortices increases with the angle of attack.

Concerning the comparison between the vortices obtained by CFD and CNN, both methods show fairly similar results in terms of vortex size. Although in both cases the previously explained vortex shapes obtained, i.e. circular for high vane-heights and elliptical for low vane-heights; the vortices obtained by CFD have a more uniform shape than those obtained by CNN, having these ones some discontinuities, especially in the outer region

(a)

(b)

(c)

Figure 9. Relative error analysis based on the distance from the TE of the VG. (**a**) Relative u_x error; (**b**) Relative u_y error; (**c**) Relative u_z error; (**d**) Relative ω_x error.

Histogam of relative ω_x error based on the plane distance

(d)

Figure 9. Continued.

of the vortex. This problem is more noticeable as the angle of attack increases.

Vortex path

In order to analyse the vortex path of the primary vortex generated by the VG, the location of the vortex centre is evaluated. As explained by Yao et al. (2022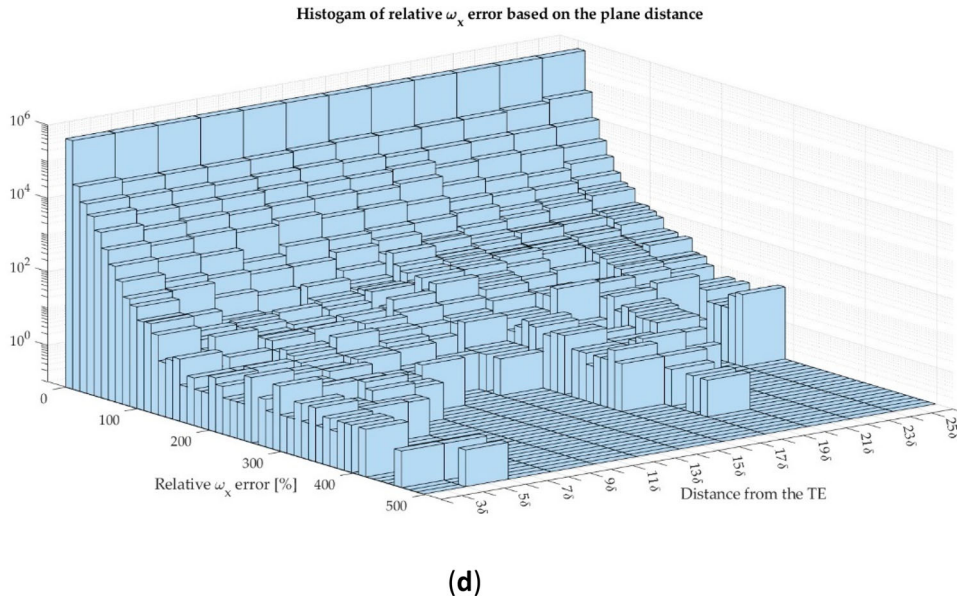), the vortex centre is the point where the peak vorticity appears. Figure 11 shows the lateral path of the primary vortex normalised with the height of each VG. Aiming to validate the obtained results with experimental data, the lateral path obtained with $\alpha = 10°, \alpha = 15°$ and $\alpha = 18°$ are compared to the data obtained experimentally by Bray (1998) for H = 0.9δ.

The lateral path obtained with CFD shows that the displacement of the main vortex increases as it distances from the VG, following an almost linear trend along the entire wake behind the VG. For all the angles of attack, the larger normalised displacements are obtained with the lower VGs, whereas the smallest ones are obtained with the higher VGs. In all the tested cases, the vortex displacement increases as the angle of attack of the VGs increase. Good agreements are obtained with the experimental data reported by Bray (1998), being the experimental samples ($H = 0.9\delta$) between the samples of $H = 0.8\delta$ and $H = 1\delta$.

The lateral path of the vortexes obtained with CNN show that the CNN is able to predict accurately the location of the vortex centre, taking the CFD results as benchmark. Nevertheless, the results obtained with CNN do not show the linear trend that those obtained with CFD

show, presenting discontinuities in some cases. This is attributed to the fact that in the predictions performed by CNN the results of the planes do not depend on the results of the previous planes, while in CFD they are dependent on them. Despite the errors that may appear, as with CFD, the larger normalised lateral displacements are obtained with the lowest vane-heights and the higher angles of attack.

Velocity profiles

As demonstrated by Velte et al. (2009), Velte (2013), the primary vortex generated by the VG possess helical symmetry, and therefore, the axial (u_x) and azimuthal (u_θ) velocity profiles are interrelated by a linear relation defined in their study. In this study both velocity components are analysed. To obtain both velocity profiles, a line that crosses the centre of the vortex is considered. Figure 12 shows the velocity profiles at a distance of 5δ from the TE of the VG obtained with both methods for each VG height and angle of attack. The velocity components are normalised with the streamwise velocity.

The axial velocity profiles show a small decrease in axial velocity at the centre of the vortex for all the vane heights. This decrease is more noticeable with the lowest vane heights and the highest angles of attack. With high angles of attack a secondary decrease in axial velocity appears, caused by the suction side of the horseshoe vortex. The azimuthal velocity profiles show an increase in azimuthal velocity followed by a decrease. This is caused by the rotation of the primary vortex, and is more noticeable in the cases with the highest angles of attack
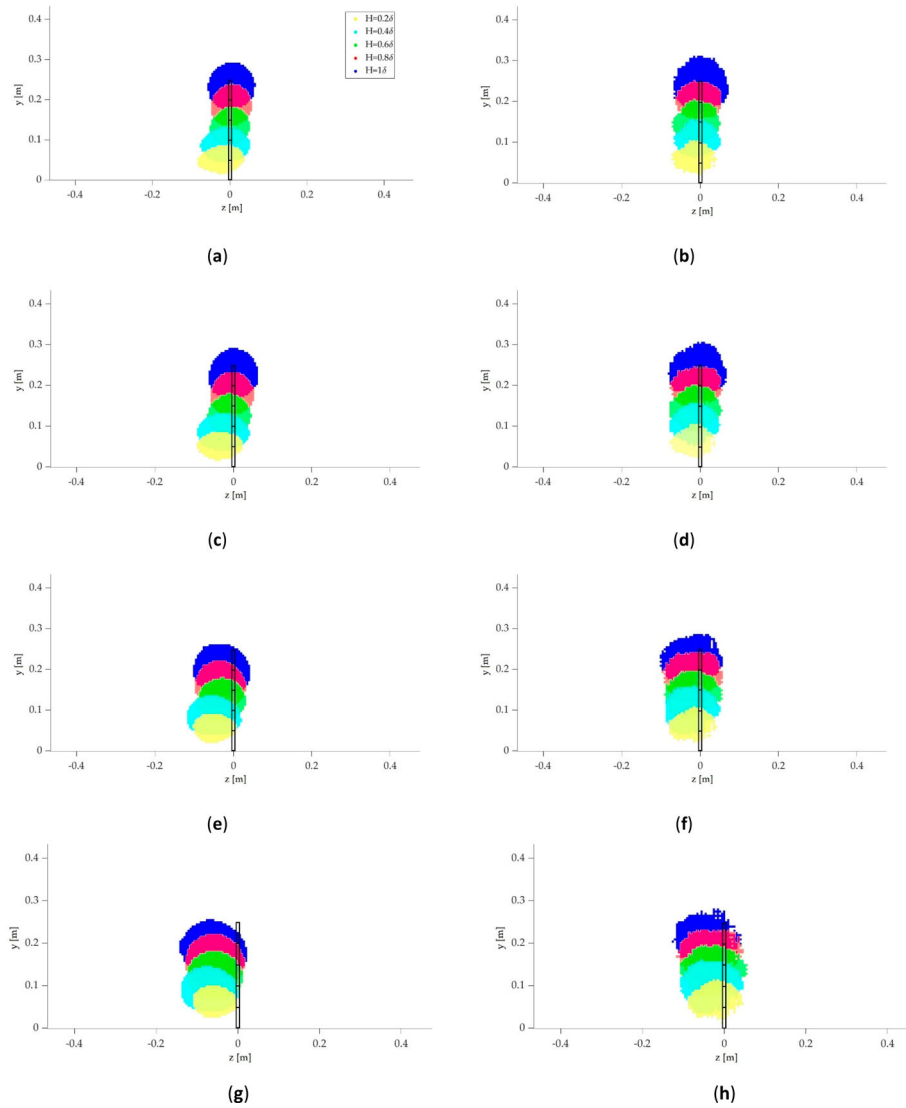
Figure 10. Vortical shape of the primary vortex at a distance of 5δ from the TE of the VG. The black rectangles represent the projection of the TE of the VGs. (**a**) $\alpha = 10°$ with CFD; (**b**) $\alpha = 10°$ with CNN; (**c**) $\alpha = 12°$ with CFD; (**d**) $\alpha = 12°$ with CNN; (**e**) $\alpha = 15°$ with CFD; (**f**) $\alpha = 15°$ with CNN; (**g**) $\alpha = 18°$ with CFD; (**h**) $\alpha = 18°$ with CNN.

and vane heights. The explained velocity profiles follow the interrelation described by Velte et al. (2009) and Velte (2013).

The CNN is able to correctly predict these velocity profiles with all the angles of attack and vane heights, showing very slight differences with respect to the CFD results.

Performance analysis

The main reason for using Deep Learning techniques instead of CFD tools is the significant reduction in computational time associated with them. Therefore, the computational time required by each of the methods to perform the predictions is a parameter to be taken into account.

To perform each CFD simulation, around 47 h were required, using 56 Intel Xeon 5420 cores with 45 GB of RAM. In contrast, 149.3 s were required to obtain the predictions of the 20 cases of the test-set, using a single core of the same processor. For training the network around 20 h were required. Table 2 shows a comparison of the average computational time required by CFD methods to obtain the results and the time required by the CNN for making the predictions of the 12 planes of a single case; moreover, the speed up of the CNN in comparison with CFD simulations is shown.

Conclusions

In this work a CNN is designed and trained to predict the velocity and vorticity fields in the wake behind vane-type
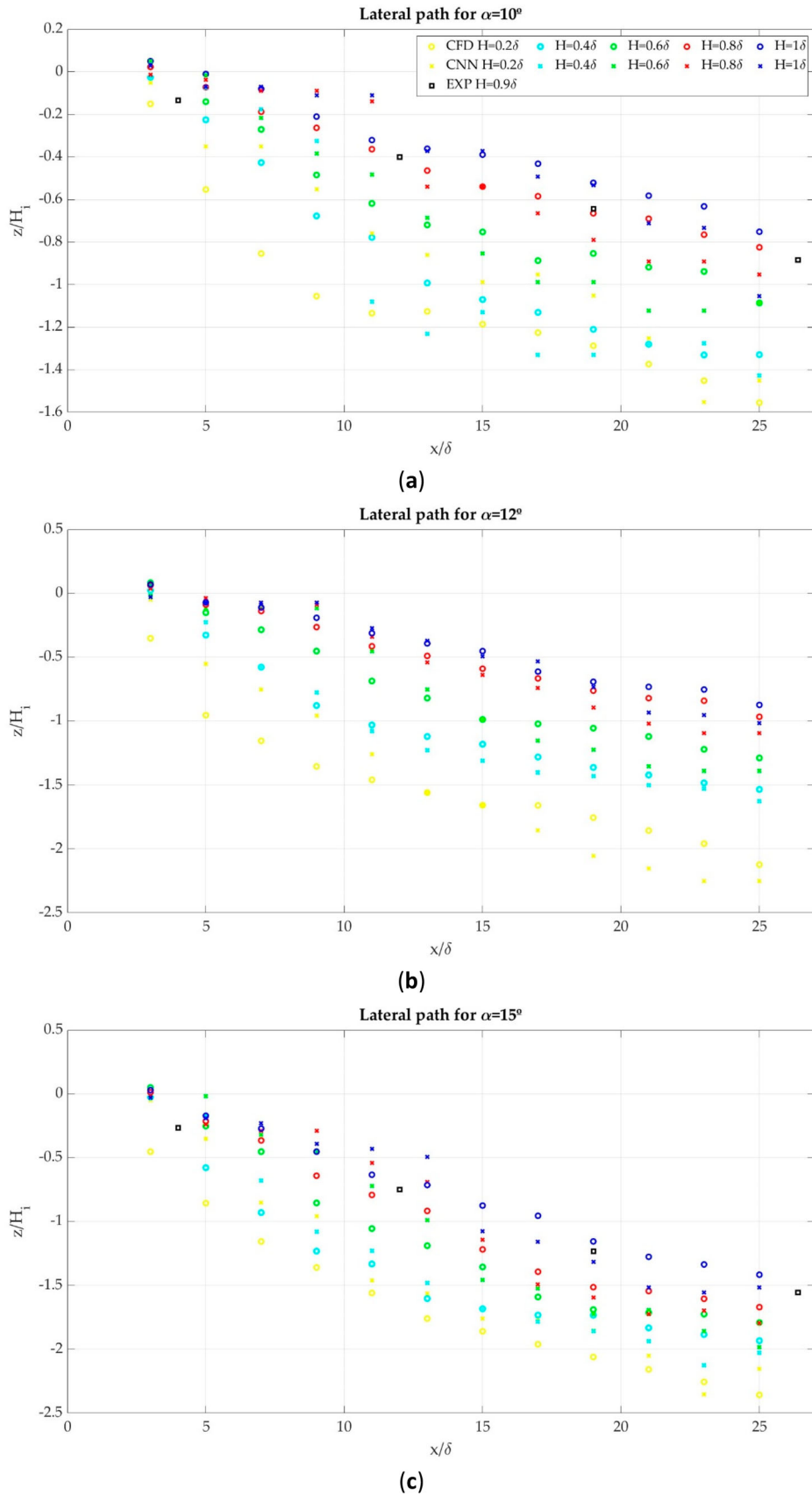
Figure 11. Comparison of the lateral path of the primary vortex. (**a**) $\alpha = 10°$; (**b**) $\alpha = 12°$; (**c**) $\alpha = 15°$; (**d**) $\alpha = 18°$.

(d)
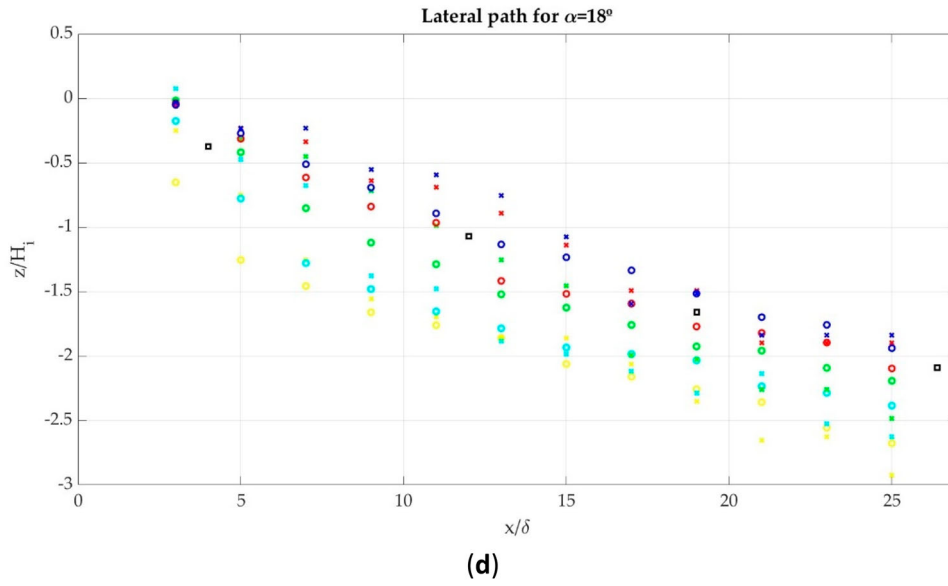
Figure 11. Continued.

(a)

(b)

(c)

(d)
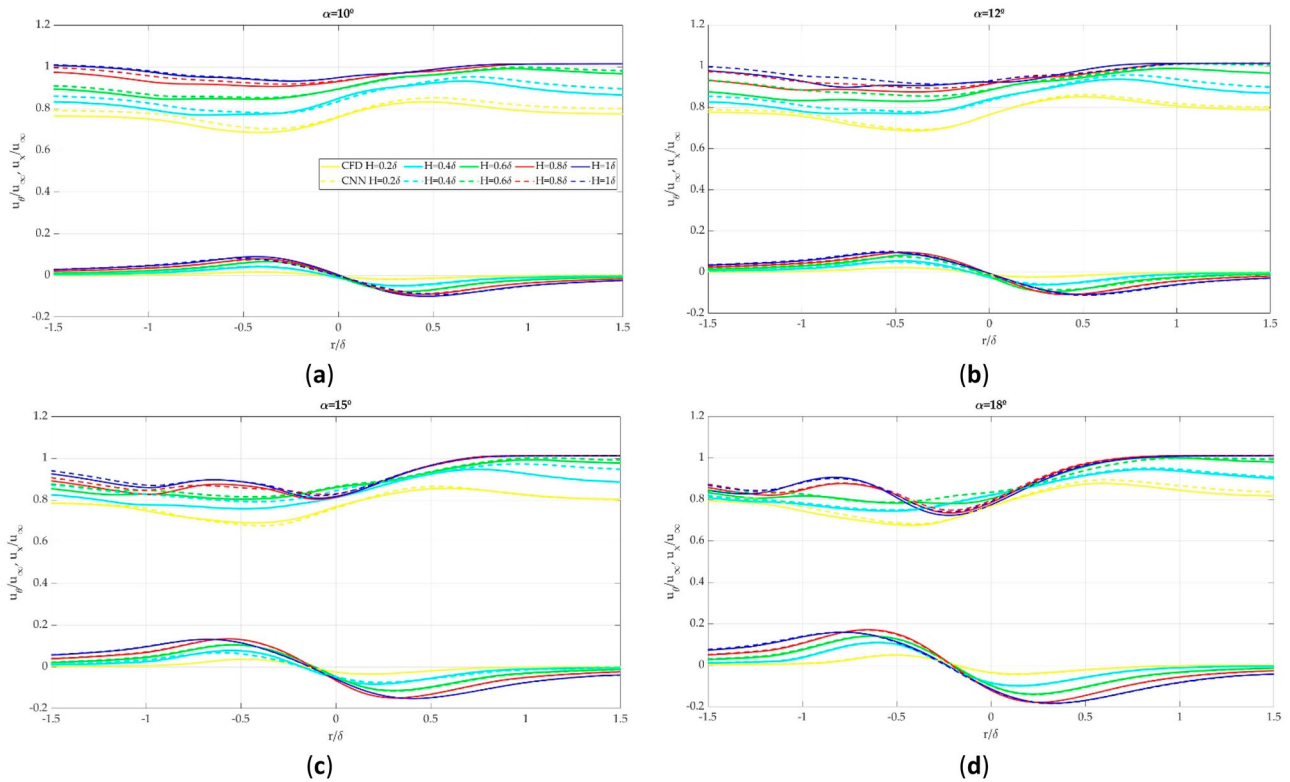
Figure 12. Velocity profiles on the vortex core at $x = 5\delta$. (**a**) $\alpha = 10°$; (**b**) $\alpha = 12°$; (**c**) $\alpha = 15°$; (**d**) $\alpha = 18°$.

Table 2. Computational time required by each method to obtain the predictions of a single case.

Method	Computational time	Speedup
CFD	47 h	–
CNN	7.465 s	22,665.77

SBVGs, aiming to study the capability of the CNN to learn and predict flow phenomena. For that purpose, 20 different CFD simulations were run, considering different angles of attack and heights of the VGs.

The results of velocity and vorticity fields show that the CNN is able to reliably predict those fields. The CNN

correctly predicts the shape of the main vortex mechanism generated by the VGs, but there are two main troubleshooting areas. The first troubleshooting area is the vortex core, where the CNN underestimates the strength of the vortex core; and the second troubleshooting area is the suction side of the horseshoe vortex, where the CNN undervalues its velocity in x direction.

With the obtained velocity and vorticity fields, an exhaustive error analysis is conducted, in order to analyse the impact of each parameter (VG height, angle of attack and distance of the plane from the TE) on the predictions carried out by the CNN. This error analysis demonstrates that the largest errors appear on the near-wake area with the taller VGs and the larger angles of attack. This is attributed to the vortical structure of the mentioned cases, since the most complex structures appear in these cases.

Additionally, the vortical structures, vortex path and velocity profiles on the vortex core are extracted from the predicted velocity and vorticity fields. The vortical structure shows that, although with some discontinuities in the outer region of the vortex core, the CNN is able to successfully predict the shape and size of the main vortex. The vortex path also demonstrates that the CNN is able to predict the vortex displacement in both trend and values. The CNN is also able to predict the velocity profiles on the vortex core very accurately.

As the main objective of using DL-based methods instead of the traditional numeric methods is to reduce the computational time, a performance analysis is conducted, in which the time required to conduct CFD simulations and CNN predictions is compared. This analysis shows a speedup of 5 orders of magnitude of the CNN in comparison with CFD simulations.

Acknowledgements

Author contributions

Conceptualisation, K.P.-P. and U.F.-G.; methodology, X. U.-G.; software, E.Z.; validation, K.P.-P. and U.F.G.; formal analysis, R.G-F.; investigation, K.P.-P.; resources, U.F.-G.; data curation, K.P.-P.; writing – original draft preparation, K.P.-P.; writing – review and editing, R.G-F.; visualisation, X. U.-G.; supervision, U.F.-G.; project administration, E.Z.; funding acquisition, U.F.-G. All authors have read and agreed to the published version of the manuscript.

Disclosure statement

Funding

Data availability statement

All data generated in the current work is available upon reasonable request to the corresponding author.

Nomenclature

CFD	Computational Fluid Dynamics
CNN	Convolutional Neural Network
DL	Deep Learning
DRL	Deep Reinforcement Learning
RANS	Reynolds-Averaged Navier–Stokes
ReLU	Rectifier Linear Unit
SBVG	Sub-Boundary-layer Vortex Generator
SDF	Signed Distance Function
SST	Shear Stress Transport
TE	Trailing Edge
VG	Vortex Generator
$*$	Dimensionless variable
$`$	Variable ranged between 0 and 1
α	Angle of Attack
Δz	First cell height
δ	Boundary layer thickness
ε_R	Relative error
H	VG height
L	VG length
Φ	Normalized magnitude
ρ	Density
Re	Reynolds number
σ	Standard deviation
u	Velocity
u_x	Axial velocity
u_θ	Azimuthal velocity
u_∞	Freestream velocity
μ	Arithmetic mean
v	Kinematic viscosity
ω	Vorticity
x, y, z	Cartesian components
Z	Zero-level set

References

Allan, B., Yao, C.-S., & Lin, J. (2002, June 24). Numerical simulations of vortex generator vanes and jets on a flat plate. In *Proceedings of the 1st flow control conference*. American Institute of Aeronautics and Astronautics.

Aramendia, I., Fernandez-Gamiz, U., Ramos-Hernanz, J. A., Sancho, J., Lopez-Guede, J. M., & Zulueta, E. (2017). Flow control devices for wind turbines. In N. Bizon, N. Mahdavi Tabatabaei, F. Blaabjerg, & E. Kurt (Eds.), *Energy harvesting and energy efficiency*. Lecture notes in energy (Vol. 37, pp. 629–655). Springer International Publishing. ISBN 978-3-319-49874-4.

Aramendia-Iradi, I., Fernandez-Gamiz, U., Sancho-Saiz, J., & Zulueta-Guerrero, E. (2016). State of the art of active and passive flow control devices for wind turbines. *DYNA*, *91*(1), 512–516. https://doi.org/10.6036/7807

Ashill, P., Fulker, J., & Hackett, K. (2001, January 8). Research at DERA on sub boundary layer vortex generators (SBVGs). In *Proceedings of the 39th aerospace sciences meeting and exhibit*. American Institute of Aeronautics and Astronautics.

Ashill, P., Fulker, J., & Hackett, K. (2002, January 14). Studies of flows induced by sub boundary layer vortex generators (SBVGs). In *Proceedings of the 40th AIAA aerospace sciences meeting & exhibit*. American Institute of Aeronautics and Astronautics.

Bray, T. P. (1998). *A parametric study of vane and air-jet vortex generators* [Ph.D. thesis]. Cranfield University, College of Aeronautics.

Chen, H., He, L., Qian, W., & Wang, S. (2020). Multiple aerodynamic coefficient prediction of airfoils using a convolutional neural network. *Symmetry*, *12*(4), 544. https://doi.org/10.3390/sym12040544

Deep Learning Toolbox. (2021). Accessed July 3, 2021, from https://es.mathworks.com/products/deep-learning.html

Du, B., Lund, P. D., & Wang, J. (2021). Combining CFD and artificial neural network techniques to predict the thermal performance of all-glass straight evacuated tube solar collector. *Energy*, *220*, 119713. https://doi.org/10.1016/j.energy.2020.119713

Fernandez-Gamiz, U., Errasti, I., Gutierrez-Amo, R., Boyano, A., & Barambones, O. (2018). Computational modelling of rectangular sub-boundary layer vortex generators. *Applied Sciences*, *8*(1), 138. https://doi.org/10.3390/app8010138

Fernandez-Gamiz, U., Marika Velte, C., Réthoré, P.-E., Sørensen, N. N., & Egusquiza, E. (2016). Testing of self-similarity and helical symmetry in vortex generator flow simulations: Self-similarity and helical symmetry in VG flow simulations. *Wind Energy*, *19*(6), 1043–1052. https://doi.org/10.1002/we.1882

Fernandez-Gamiz, U., Réthoré, P.-E., Sørensen, N. N., Velte, C. M., Frederik, Z., & Egusquiza, E. (2012, March 16). *Comparison of four different models of vortex generators*. European Wind Energy Association (EWEA).

Guo, X., Li, W., & Iorio, F. (2016, August 13). Convolutional neural networks for steady flow approximation. In *Proceedings of the proceedings of the 22nd ACM SIGKDD international conference on knowledge discovery and data mining* (pp. 481–490). ACM.

Ibarra-Udaeta, I., Portal-Porras, K., Ballesteros-Coll, A., Fernandez-Gamiz, U., & Sancho, J. (2020). Accuracy of the cell-set model on a single vane-type vortex generator in negligible streamwise pressure gradient flow with RANS and LES. *Journal of Marine Science and Engineering*, *8*(12), 982. https://doi.org/10.3390/jmse8120982

Jacob, S. J., Mrosek, M., Othmer, C., & Köstler, H. (2022). Deep learning for real-time aerodynamic evaluations of arbitrary vehicle shapes. *SAE International Journal of Passenger Vehicle Systems*, *15*(2), 77–90. https://doi.org/10.4271/15-15-02-0006

Kashefi, A., Rempe, D., & Guibas, L. J. (2020). A point-cloud deep learning framework for prediction of fluid flow fields on irregular geometries. *ArXiv201009469 Phys*.

Kingma, D. P., & Ba, J. (2017). Adam: A method for stochastic optimization. *ArXiv14126980 Cs*.

MATLAB. (2022). Accessed June 9, 2021, from https://es.mathworks.com/products/matlab.html

Menter, F. (1993, July 6). Zonal two equation K-w turbulence models for aerodynamic flows. In *Proceedings of the 23rd fluid dynamics, plasmadynamics, and lasers conference*. American Institute of Aeronautics and Astronautics.

Portal-Porras, K., Fernandez-Gamiz, U., Aramendia, I., Teso-Fz-Betoño, D., & Zulueta, E. (2021a). Testing the accuracy of the cell-set model applied on vane-type sub-boundary layer vortex generators. *Processes*, *9*(3), 503. https://doi.org/10.3390/pr9030503

Portal-Porras, K., Fernandez-Gamiz, U., Ugarte-Anero, A., Zulueta, E., & Zulueta, A. (2021b). Alternative artificial neural network structures for turbulent flow velocity field prediction. *Mathematics*, *9*(16), 1939. https://doi.org/10.3390/math9161939

Portal-Porras, K., Fernandez-Gamiz, U., Zulueta, E., Ballesteros-Coll, A., & Zulueta, A. (2022). CNN-Based flow control device modelling on aerodynamic airfoils. *Scientific Reports*, *12*(1), 8205. https://doi.org/10.1038/s41598-022-12157-w

Qi, C. R., Su, H., Mo, K., & Guibas, L. J. (2017). *PointNet: Deep learning on point sets for 3D classification and segmentation* (pp. 652–660).

Ren, J., Wang, H., Luo, K., & Fan, J. (2021). A priori assessment of convolutional neural network and algebraic models for flame surface density of high Karlovitz premixed flames. *Physics of Fluids*, *33*(3), 036111. https://doi.org/10.1063/5.0042732

Ribeiro, M. D., Rehman, A., Ahmed, S., & Dengel, A. (2020). DeepCFD: Efficient steady-state laminar flow approximation with deep convolutional neural networks. *ArXiv200408826 Phys*.

Ronneberger, O., Fischer, P., & Brox, T. (2015). U-Net: Convolutional networks for biomedical image segmentation. In N. Navab, J. Hornegger, W. M. Wells, & A. F. Frangi (Eds.), *Proceedings of the medical image computing and computer-assisted intervention – MICCAI 2015* (pp. 234–241). Springer International Publishing.

Thuerey, N., Weißenow, K., Prantl, L., & Hu, X. (2020). Deep learning methods for Reynolds-averaged Navier–Stokes simulations of airfoil flows. *AIAA Journal*, *58*(1), 25–36. https://doi.org/10.2514/1.J058291

Urkiola, A., Fernandez-Gamiz, U., Errasti, I., & Zulueta, E. (2017). Computational characterization of the vortex generated by a vortex generator on a flat plate for different vane angles. *Aerospace Science and Technology*, *65*, 18–25. https://doi.org/10.1016/j.ast.2017.02.008

Velte, C. M. (2013). A vortex generator flow model based on self-similarity. *AIAA Journal*, *51*(2), 526–529. https://doi.org/10.2514/1.J051865

Velte, C. M., Hansen, M. O. L., & Okulov, V. L. (2009). Helical structure of longitudinal vortices embedded in turbulent wall-bounded flow. *Journal of Fluid Mechanics*, *619*, 167–177. https://doi.org/10.1017/S0022112008004588

Velte, C. M., Hansen, M. O. L., & Okulov, V. L. (2016). Multiple vortex structures in the wake of a rectangular winglet in ground effect. *Experimental Thermal and Fluid Science*, *72*, 31–39. https://doi.org/10.1016/j.expthermflusci.2015.10.026

Yao, C., Lin, J., & Allen, B. (2022). Flowfield measurement of device-induced embedded streamwise vortex on a flat plate. In *1st Flow control conference*. American Institute of Aeronautics and Astronautics.

Yilmaz, E., & German, B. (2017). A convolutional neural network approach to training predictors for airfoil performance. In *18th AIAA/ISSMO multidisciplinary analysis and optimization conference*. American Institute of Aeronautics and Astronautics.

Zhang, Y., Sung, W. J., & Mavris, D. N. (2018). Application of convolutional neural network to predict airfoil lift coefficient. In *2018 AIAA/ASCE/AHS/ASC structures, structural dynamics, and materials conference*. American Institute of Aeronautics and Astronautics.